Electrical Power and Energy Systems 148 (2023) 108986

Contents lists available at ScienceDirect

International Journal of Electrical Power and Energy Systems

journal homepage: www.elsevier.com/locate/ijepes

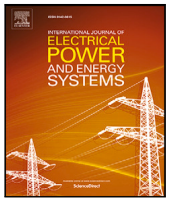

Distributed consensus-based secondary control of multi-terminal DC railway systems

J. Carlos Olives-Camps, Juan Manuel Mauricio, José María Maza-Ortega *, Antonio Gómez-Expósito

Department of Electrical Engineering, Universidad de Sevilla, Camino de los Descubrimientos s/n, 41092, Seville, Spain

ARTICLE INFO

Keywords:
Distributed cooperative control
Medium-voltage DC (MVDC)
Multi-terminal DC (MTDC)
Railway electrification
Secondary voltage control

ABSTRACT

Electrification of the transportation sector is one of the main pillars of the future decarbonized society. In this context, high-speed railway corridors are expected to reduce as much as possible their environmental impact while maintaining the safety and quality of service with minimum investments. In pursuing those objectives, the multi-terminal DC railway system may become the preferred paradigm. In contrast to conventional AC railway electrification schemes, the multi-terminal DC railway system requires the adoption of a control algorithm to establish suitable references for the power converters. This paper elaborates on a new consensus-based secondary control strategy, which can be implemented in a distributed fashion. In this approach, each power converter controller receives information from its nearest neighbors to adjust its operating point. A 600-km railway system, subject to realistic train traffic, is used to compare the performance of the proposed control strategy with that of purely local controllers. Numerical simulations evidence that the proposed distributed control scheme provides a compromise solution in terms of voltage drops and equalization of power converter loading, surpassing the performance of conventional state-of-the art controllers.

1. Introduction

Electric railways are expected to play an important role in the coming decades in decarbonizing the transportation system. According to [1], the global demand for passenger and freight transport is expected to double by 2050. The main expected actors in this arena are China, India, Europe, and Russia, making this issue a matter of global interest. Therefore, it becomes essential to improve the efficiency while at the same time reducing the investment and operating costs of these transportation systems.

Currently, several AC and DC railway electrification arrangements coexist, each with its own layout of rolling stock, catenaries, and feeding substations. Traditionally, DC systems have been restricted to trams, commuter trains, and medium-distance trains [2] with voltages lower than 3 kV. In contrast, single-phase high-voltage AC systems are employed for long-distance and high-speed trains due to the higher power demand of these traction applications [3]. Although they have been around for decades, both distinct and disjoint electrification arrangements are quite mature. However, the advent of the IGBT-based Voltage Source Converter (VSC) is expected to drastically and quickly change the landscape, giving rise to several new applications aimed at improving the performance of those traditional feeding technologies [4]. For example, the possibility of downsizing the AC substation, resorting to the so-called Hybrid Railway Power Conditioner (HRPC), is presented in [5]. Furthermore, [6–10] also explore the benefits that the incorporation of distributed resources, including renewable generation and energy storage systems, can provide in terms of environmental impact. In this line, an interesting discussion about the location of the storage system, the reversibility of the feeding substations, and the regenerative braking of the rolling stock is analyzed in [11]. It is also possible to find applications to improve power quality by compensating harmonics and imbalances in single-phase AC systems [12–14].

In fact, VSC technology has made the break-even point between AC and DC systems no longer clear [15]. It was recognized early in [16] that single-phase AC is not the ideal railway electrification system, as DC schemes may bring important advantages. Following this line, [17] proposes a brand new electrification system entirely built around a seamless medium voltage DC (MVDC) catenary, supplied from the AC grid by a number of VSC, conforming in this way a multi-terminal DC (MTDC) system. This new paradigm also considers the possibility of interconnecting multiple traction subsystems, each with different DC voltage levels, which are mainly determined by the expected power density of the transportation route. Such an MTDC railway scheme would eventually bring a number of benefits, particularly in greenfield

* Corresponding author.
E-mail address: jmmaza@us.es (J.M. Maza-Ortega).

https://doi.org/10.1016/j.ijepes.2023.108986
Received 2 August 2022; Received in revised form 29 December 2022; Accepted 16 January 2023
Available online 1 February 2023

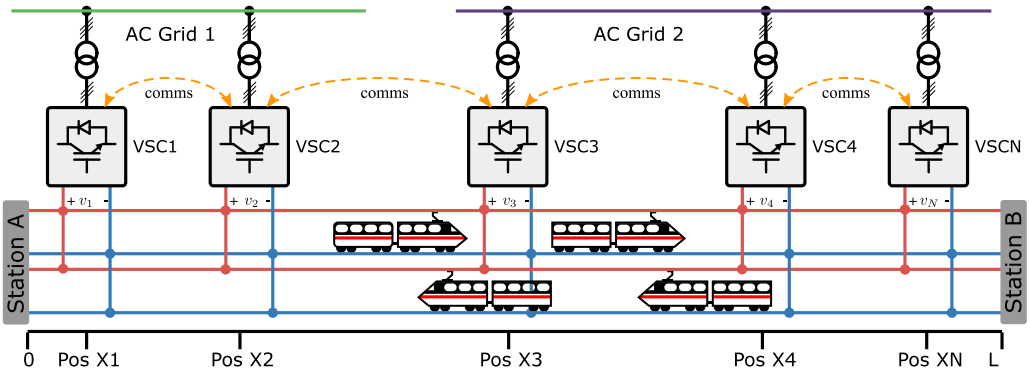

Fig. 1. DC railway system fed by N power stations.

developments, ranging from simpler rolling stock layouts, reduced investment in railway infrastructure, higher reliability and modularity, more friendly integration into the AC grid, and opportunities for new business models.

The control approach for this new railway electrification system, as outlined in [17], relies on a hierarchical control system similar to those used in conventional AC and DC power systems: a central supervisory (secondary) controller coordinates the local (primary) VSC controllers, so that the resulting power flows are optimized while the DC voltage is kept within limits throughout the catenary length. In this sense, several alternatives can be considered regarding coordinated control of DC voltage for multi-terminal VSC-MVDC distribution networks [18]. In [19,20], custom droops are proposed for the primary controllers of MTDC systems to improve the power-sharing among the converters connected to the DC network. In [21] the classic primary, secondary, and tertiary hierarchical approach is considered for AC and DC microgrids, in this case involving a centralized secondary controller that requires dedicated communication links with each individual primary controller. In [22], a sparse communication network is unfolded across an AC microgrid to facilitate limited data exchange among inverter controllers, satisfying primary and secondary control objectives. In [23], a communication network is proposed to improve the current sharing capabilities of a railway system. However, the main drawback of this method is that it requires the addition of voltage measurement points that communicate with power substations.

In this paper, a distributed semi-autonomous voltage/power control for MTDC railway systems is proposed in which VSC local controllers exclusively exchange information with their direct neighbors. The design of the controller is based on the framework of multi-agent systems. Among its advantages is the fact that it is not based on the plant model, but on the measurements, so that the inclusion of exogenous variables does not affect the performance of the controller. The performance and ratings of the proposed approach are compared with those of two customary fully autonomous local control strategies, namely: (a) fixed voltage strategy, (b) unsupervised local droop controller.

The paper is structured as follows: Section 2 provides a brief overview of the MTDC railway system. Section 3 reviews customary autonomous control strategies. Section 4 presents the proposed control strategy. Section 5 provides simulation results showing the benefits of the proposed load-sharing method. Conclusions are drawn in Section 6.

2. DC railway system

Fig. 1 shows the topology of the MTDC railway system proposed in [17] to connect train stations A and B. The railway system may conceptually be thought of as a single DC catenary running without interruption from A to B, fed by a number of power stations at intermediate points. One of the main advantages of this new electrification paradigm for railways is that the total installed power of power stations is much lower than that of conventional AC systems with split catenaries [17]. The following subsections provide some details about the power stations and the communication infrastructure required to implement the proposed control scheme.

2.1. Converters station model

In the MTDC paradigm, each power station is composed of a VSC connected to a high-voltage AC system through a power transformer, as shown in Fig. 1. This has several advantages from the point of view of the AC system. On the one hand, the power demanded by the railway system is balanced, unlike in single-phase AC electrification schemes. On the other hand, it is possible to operate at the unity power factor, making the use of reactive power compensators unnecessary.

Taking into account the power and voltage levels involved, the suitable VSCs for this application are Modular Multilevel Converters (MMC) [24,25]. MMC VSCs are characterized by high conduction losses and very low switching losses due to their low switching frequency [26], so it is possible to neglect the loss term that depends linearly on the DC current of the VSC. As a consequence, the total power losses to be considered in the VSC power station can be expressed as follows:

$$p_{loss} = A_{loss} i_{dc}^2 + B_{loss}, \tag{1}$$

where $i_{dc} = p_{dc}/v_{dc}$, A_{loss} is a parameter that accounts for VSC and transformer conduction losses and B_{loss} models the no-load losses that include: switching losses, transformer no-load losses, VSC and transformer cooling system losses, filter losses, and auxiliary services.

2.2. Communication infrastructure

The MTDC railway system can be operated in several ways, depending on the available communication infrastructure. In the seminal work in which this concept was proposed, two control strategies were envisioned [17]. In the simplest approach, the target of each VSC is to maintain its DC output voltage constant, which is termed in this paper as Fixed Voltage approach (discussed in detail later). The second one is based on a centralized supervisory controller, intended to optimize the DC output of the VSCs according to a given criterion. Note that this second approach requires a communication infrastructure connecting all substations to the central controller. If public communication networks were used, this would result in high exposure to cyber attacks. In addition, any outage of the central controller may significantly compromise the overall system performance.

To overcome those shortcomings, this work proposes a distributed control strategy, i.e. without a centralized controller, involving a simpler and more resilient communication infrastructure. Communication links are deployed exclusively between adjacent VSC power stations, as shown in Fig. 1, closely resembling the arrangement proposed in [27] for microgrids. Due to the typical distances involved between the power stations, and the very low bandwidth required, low-cost technologies, such as Power Line Communication (PLC), can be safely used [28].

3. Local control strategies

A suitable control strategy for power systems based on electronic-interfaced power supplies should focus on the following objectives [29]:

(a) Equalization of the shared load per unit among the sources.
(b) Ensure voltage regulation throughout the system.

Despite the advantages of simple control systems, which are exclusively based on local measurements, the conventional strategies discussed in the following subsections fail to satisfy both objectives simultaneously.

3.1. Fixed voltage controller

The simplest VSC control strategy in charge of feeding the DC system is to keep its own DC output voltage at a given reference value as follows:

$$v_i^\star = V^0, \tag{2}$$

where V^0 is a constant value and $v_i^\star$ is the reference voltage on the DC side of the VSC i. Note that the VSCs shown in Fig. 1 are equipped with fast controllers capable of maintaining the DC side voltage at the desired value regardless of load changes or other perturbations. This means that $v_i \to v_i^\star$ in a few milliseconds. This very simple strategy is the most effective in terms of the minimal current flowing along the catenary. Consequently, Joule losses are reduced. However, this strategy does not satisfy the load-sharing requirement among converters, resulting in unnecessarily high converter oversizing.

3.2. Voltage droop controller

Load-sharing among generators has traditionally been a crucial problem in AC power systems. For this purpose, a real power–frequency (P-f) droop characteristic has usually been implemented in the primary generator controllers [30]. Despite being a purely local control law, its application guarantees a global and almost perfect load-sharing between generators. The effectiveness of this simple control action in AC power systems is based on the following facts:

(a) The frequency is a global variable of the steady-state power system.
(b) The real power flows between two nodes of the system depend mainly on the relative angles of their nodal voltages.
(c) The angle of any generator voltage depends on the integral of frequencies.

Taking into account (a), each generator of the power system can *observe* any imbalance between generation and demand, regardless of how far it is from the rest of the generators. In case of an imbalance, and considering (b) and (c), the angles will change until almost perfect load-sharing is achieved. This is because the angles are the integral of the frequency; therefore, their behavior is similar to that of a PI controller.

However, in a DC system, there is no frequency or angle. Power flows depend only on voltage magnitude differences between generators and loads. Therefore, instead of a P–f droop, a power–voltage (P–V) droop is customarily applied. Thus, an alternative strategy to set the VSC DC output voltage can be stated as follows:

$$v_i^\star = V^0 - K_r p_i, \tag{3}$$

where p_i is the active power measured at the terminals of VSC i and K_r is the positive droop coefficient.

However, the application of this simple strategy has several drawbacks compared to its AC counterpart:

(a) The voltage is a local magnitude.
(b) Perfect load-sharing is impossible among distant generators.
(c) Large droops are required in those cases, causing severe voltage variations.

Taking into account (a), the ability of any generator to detect any imbalance between generation and demand is drastically reduced. Therefore, it is very difficult for far away generators to collaborate in sharing the load in an efficient manner, as stated in point (b). A possible improvement of this undesirable situation can be achieved by using large droops, leading to undervoltages or overvoltages, as pointed out in (c). In addition, those large droops can be seen as large gains in closed-loop control, increasing the risk of making the entire system unstable [31]. For this reason and in order to satisfy both requirements defined at the beginning of this section, a secondary control layer must be implemented to adjust the setpoints of the primary control layer. Recently, in [32], it was proposed that a centralized controller modifies the droop parameter to define the cooperation between the traction substations. However, the limitations of this scheme are related to the reliability of communications and the computational cost of central processing.

4. Secondary voltage control based on a distributed cooperative scheme

This section is devoted to describing the proposed distributed secondary control scheme as an alternative to a fully centralized approach. The proposal takes advantage of the underlying MTDC electrification topology for the deployment of a peer-to-peer communication infrastructure between neighboring feeding substations, as shown in Fig. 1. Such distributed approach significantly reduces the investment in communications infrastructure, as compared with a centralized controller.

In this section, a brief review of graph theory and distributed averaging algorithms is provided. Then, the consensus-based voltage droop control is presented.

4.1. Preliminaries of graph theory

Let us denote a graph as $\mathcal{G} = (\mathcal{N}, \mathcal{E}, \mathcal{A})$ with $\mathcal{N} = \{n_1, \dots, n_N\}$ being a non-empty finite set of N nodes, $\mathcal{E} \subseteq \mathcal{N} \times \mathcal{N}$ the set of communication links, and $\mathcal{A}$ the weighted adjacency matrix. The latter is defined by $a_{ii} = 0$, and $a_{ij} > 0$ if $(j,i) \in \mathcal{E}$. The neighbors of agent i are denoted by $I = \{j \in \mathcal{N} : (i,j) \in \mathcal{E}\}$. In this particular work, $\mathcal{N}$ corresponds to VSC-based substations that are permanently connected through a communication link with their corresponding neighbors. For this reason, a time-invariant graph is assumed. In addition, the graph is undirected because $a_{ij} = a_{ji}, \forall i,j$. Every undirected graph has an associated Laplacian matrix $\mathbf{L}$, characterizing its topology as follows [33]:

$$L_{ij} = \begin{cases} \sum_{j=1}^{N} a_{ij} & \text{if } i = j \\ -a_{ij} & \text{if } i \neq j. \end{cases} \tag{4}$$

It is worth noting that $\mathbf{L}$ is symmetric for undirected graphs, and therefore all of its eigenvalues are real and can be sorted in ascending order as:

$$0 = \lambda_1 \leq \lambda_2 \leq \cdots \leq \lambda_N. \tag{5}$$

The right eigenvector associated with the first zero eigenvalue is the unity vector, $\alpha\mathbf{1}$ for $\alpha \in \mathcal{R}$. For this reason, it can be shown that all elements of an arbitrary vector $\mathbf{x}$ must be the same to satisfy $\mathbf{Lx} = \mathbf{0}$ [34].

4.2. Continuous-time distributed averaging

The communication network of a multi-agent system can be modeled by an undirected and weighted graph $\mathcal{G} = (\mathcal{N}, \mathcal{E}, \mathcal{A})$ which has the

properties outlined in the previous section. Consider that each agent $i \in \{1, \dots, N\}$ has a scalar value x_i assigned. A widely used update rule for the agent i to adjust its value x_i is as follows:

$$\dot{x}_i = \sum_{j \in I} a_{ij} \left(x_j - x_i \right), \tag{6}$$

where $j \in I$ denotes the set of neighbors of node i, and a_{ij} is the corresponding value of the adjacency matrix $\mathcal{A}$. Thus, the variable x_i evolves towards a weighted average of the values of its neighbors x_j. The collective dynamics following protocol (6) can be written in terms of the Laplacian matrix as:

$$\dot{\mathbf{x}} = -\mathbf{L}\mathbf{x}. \tag{7}$$

Therefore, if the communication network $\mathcal{G} = (\mathcal{N}, \mathcal{E}, \mathcal{A})$ is active, the steady-state resulting from this dynamic process ($\mathbf{0} = -\mathbf{L}\mathbf{x}$) is such that all components of $\mathbf{x}$ converge to a common value, due to the properties of the Laplacian matrix [34]. For this reason, (6) is called continuous-time distributed averaging or consensus.

4.3. Voltage regulation and power-sharing

The fundamental idea of this work is to apply the distributed cooperative control theory to design a controller that simultaneously improves voltage regulation and power-sharing between converter stations. To ensure a proper operation, even under a communication failure scenario, it is assumed that a slightly modified primary droop controller (3) is locally implemented in all the feeding VSCs. Basically, an additional secondary control variable ξ is added to (3) as follows:

$$v_i^\star = V^0 - K_r p_i + \xi_i. \tag{8}$$

The aim of the secondary control variable ξ is to eliminate terminal voltage deviations while maintaining a proper level of power-sharing. Therefore, the secondary control law proposed in this work simultaneously considers voltage deviations from a reference value V^0, and power-sharing among neighboring VSCs, as follows:

$$\dot{\xi}_i = K_s (V^0 - v_i^\star) + \sum_{j \in i} a_{ij} (p_j - p_i), \tag{9}$$

where K_s and a_{ij} are positive gains weighting the relative importance of the pursued control objectives, a_{ij} being the (i,j)th element of the adjacency matrix $\mathbf{A}$ associated with the deployed communication network. Note that K_s is not the classical pinning gain associated to leader consensus strategies [34] because the consensus variable, p_i, and the regulation variable, $v_i^\star$, are different.

Fig. 2 shows the complete control scheme for the hth VSC and its gth and kth neighbors. The primary control layer is composed of the droop controller, to avoid overloading, while the secondary controller (9) achieves a tunable compromise between the objectives. Thus, it is possible to differentiate three cases depending on the values of these parameters:

- Case 1 ($K_s \neq 0, \mathbf{A} = 0$). In this case, the second term in (9) vanishes. As a consequence of the integral characteristic of the secondary layer, the steady state is reached when all the VSCs satisfy the condition $V^0 = v_i^\star$. Note that this behavior corresponds to the Fixed Voltage Controller (2).
- Case 2 ($K_s = 0, \mathbf{A} \neq 0$). The first term of (9) disappears in this case. Therefore, the steady state is achieved when $p_i = p_j$ for all the neighboring VSCs that feed the railway. The secondary control variables ξ converge to a value that changes the individual droop characteristic to establish perfect power-sharing.
- Case 3 ($K_s \neq 0, \mathbf{A} \neq 0$) In this case, the joint operation of (8) and (9) reaches a compromise solution between power-sharing and voltage regulation based on the relative weighting gains a_{ij} and K_s.

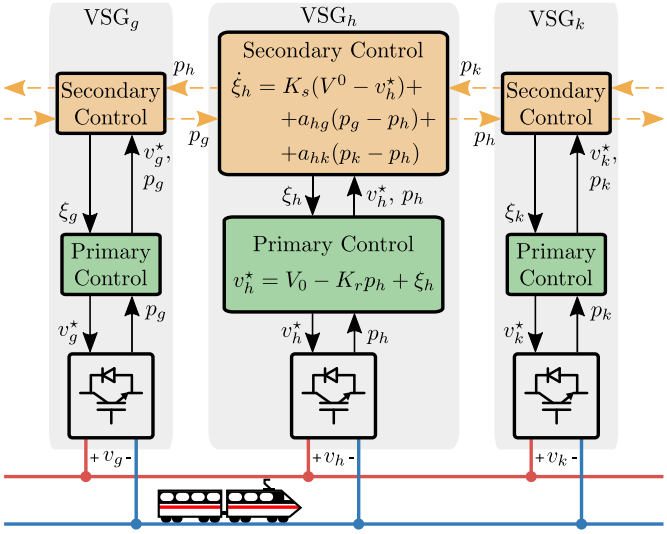

Fig. 2. Proposed secondary control strategy and communications infrastructure.

Table 1
Simulation parameters for the case study.

VSC locations	
VSC 1 (km)	60
VSC 2 (km)	180
VSC 3 (km)	300
VSC 4 (km)	420
VSC 5 (km)	540
VSC losses and efficiency	
Full-load losses (%)	1.7
No-load losses (%)	0.7
Catenary	
Cross section (mm^2)	150
Equivalent resistance mΩ/km	57
Rated voltage (kV)	24
Minimum voltage (kV)	18
Controller parameters	
K_r	0.1
K_s	2.7
a_{ij}	0.1

5. Performance assessment

This section is devoted to evaluating the performance of the proposed distributed control strategy in a railway system as depicted in Fig. 1. That is, a 600-km system is supplied from five VSC substations with the static data shown in Table 1. The simulated traffic scheduling between stations A and B is shown in Fig. 3(a). It consists of a time window from 6:00 am to 12:00 pm with five trains departing from stations A and B. Note that each train follows a trajectory conditioned by maximum speeds, arrival time, altitude changes, etc. It has been considered that all trains follow the same speed profile, which is shown in Fig. 3.(b) along with the corresponding power demand. Due to the slope of the terrain, the power consumption of the routes A-B (red curves), and B-A (green curves) are not exactly the same.

Note that the distance between the supplying VSC stations doubles the one used in conventional AC 2 × 25 kV railway electrification. This parameter has been selected in this way to highlight one of the main advantages of the multi-terminal DC paradigm, as reported in [17]. Evidently, the definition of the distance between the substations has to be determined by a planing tool which is out of the scope of this paper. In any case, it is important to highlight that the simulation results evidence that the technical constraints, i.e. minimum catenary voltages,

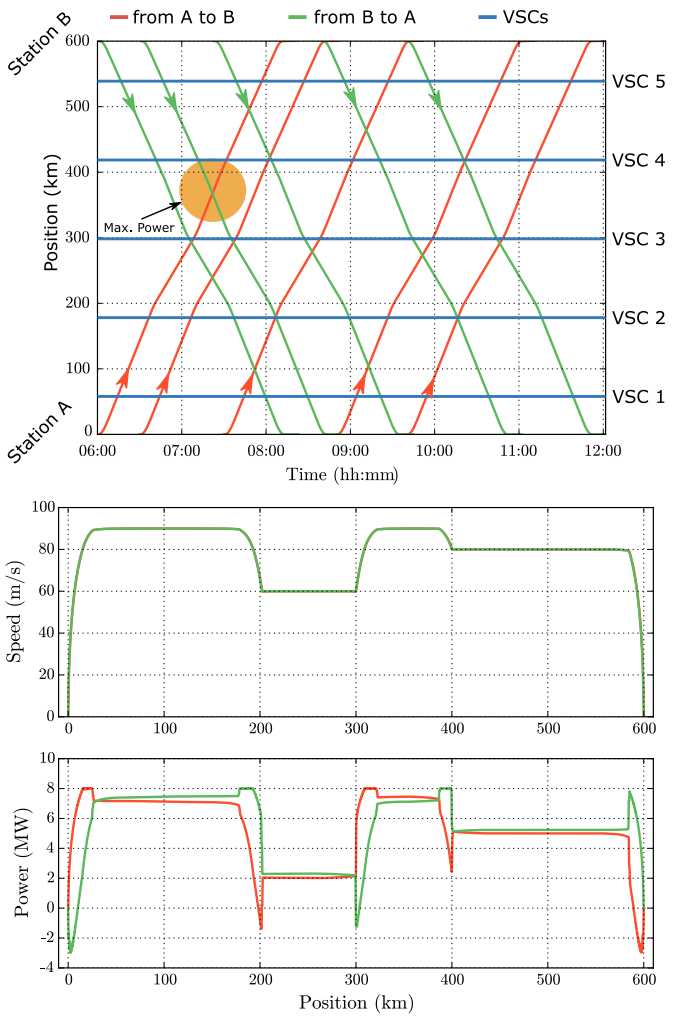

Fig. 3. (a) Traffic schedule between stations A and B. (b) Speed and power profiles along the route.

are satisfied even with this large distance between the substations. Moreover, and regarding safety issues, the rail potential and stray currents are within the regulatory limits [35]. In this respect, it has been assumed that the railway system is isolated from the ground. An estimation of the rail potential and the stray current can be done by assuming the most unfavorable position of a train, which is the mid point between two VSC substations according to [35]. With the train located at that point, the rail potential and stray current reach 77.23 V and 1.26 mA/m respectively, well below the recommended limits of 90 V and 2.5 mA/m.

Table 1 also details the catenary data and the VSC losses, duly justified in the appendix. Finally, the control parameters (K_s and a_{ij}) used in the simulations are provided. Those parameters play a key role in the performance of the consensus-based secondary control, aimed at achieving a compromise solution between the voltage regulation and power sharing. For this reason, in order to assess the influence of these parameters, a sensitivity analysis has been included at the end of this section.

The performance of the proposed distributed controller (*CONS*) is compared to those obtained by local strategies: fixed voltage (*FV*) and local droop (*LD*). For this purpose, the following set of key performance indicators (KPIs) has been selected for a quantitative and systematic comparison:

- Minimum voltage along the catenary.
- Maximum power injected by VSC substations in normal and faulted situations.
- Energy losses and efficiency of the entire system.

Two scenarios have been simulated: normal operation (i.e., all substations operating normally) and single substation failure. Note that the most critical situation corresponds to a failure in those substations with only one neighbor (VSC1 or VSC5). In this case, the nearest substation (VSC2 or VSC4, respectively) must cope with the largest catenary section, which may face under-voltage conditions.

Finally, it is worth mentioning that the secondary controller is implemented in the discrete-time domain. Therefore, to carry out the simulations, (9) is discretized using the forward Euler method with a time step of 100 ms. In addition, to model the impact of the communications delay, the active powers demanded by the neighbor VSC stations are collected with a delay with respect to the local measured magnitudes, as follows:

$$\xi_i^{\tau+1} = \xi_i^{\tau} + \Delta t \left(K_s (V^0 - v_i^{\star\,\tau}) + \sum_{j \in i} a_{ij} (p_j^{\tau-1} - p_i^{\tau}) \right), \tag{10}$$

where Δt represents the delay considered and τ the discrete time step.

5.1. Normal operation

The voltage profiles along the catenary for the simulated period are compared in Fig. 4. Due to the displacement of trains, the voltage profile is continuously changing (red color is used to highlight the time instant when the minimum catenary voltage is reached). An initial analysis of these curves evidences the inherently opposite behavior of the local controllers *FV* and *LD*. Note that the *FV* control strategy leads to the minimum voltage variations along the catenary, as the VSC stations maintain the supply voltage to a constant value. On the contrary, the *LD* controller yields the highest voltage variations, since the objective is to equalize the traction load as much as possible, irrespective of the supply voltage. In contrast, the proposed secondary, consensus-based controller achieves an intermediate performance, that better balances the two contradicting goals of the purely local controllers. This qualitative analysis is confirmed with a quantitative comparison taking into account the statistical data shown in Table 2. Both Fig. 4 and Table 2 clearly evidence that the best voltage regulation is obtained with the *FV* approach, with a minimum voltage around 22.91 kV (0.95 p.u.) and all voltages remaining within 23.52 kV (0.98 p.u.) and 24.25 kV (1.01 p.u.) 95% of the time. The voltage regulation clearly deteriorates in the case of the local droop controller *LD*, which leads to a minimum voltage of 20.9 kV (0.87 p.u.) and a much wider voltage range during 95% of time, namely between 21.91 kV (0.91 p.u.) and 24.13 kV (1.01 p.u.). The proposed consensus-based control technique (*CONS*) yields excellent results, with a minimum voltage of 22.54 kV (0.94 p.u.), quite close to that obtained with the *FV* approach. Additionally, the voltage range along the catenary is narrower, varying between 23.38 kV (0.97 p.u.) and 24.43 kV (1.02 p.u) 95% of the time. Therefore, taking into account the catenary voltage profile, it can be stated that the proposed *CONS* approach performs almost the same as the *FV* controller, which is the best possible control algorithm for this KPI.

The above analysis can be complemented by analyzing the VSC DC output voltages over the simulated period, as shown in Fig. 5 using box plots. As expected, voltages are kept constant in the first case, while there is a wide range of variation associated with the *LD* approach. This result suggests the need for a coordinated control strategy, implemented either centrally or in a distributed fashion, to keep the voltage range within acceptable limits. The application of the proposed *CONS* approach clearly leads to an improved voltage scenario. On the one hand, the median voltage value is close to the constant voltage used in the *FV* approach. On the other hand, the interquartile range is narrower than in the *LD* controller, which clearly demonstrates the improvement achieved in voltage regulation.

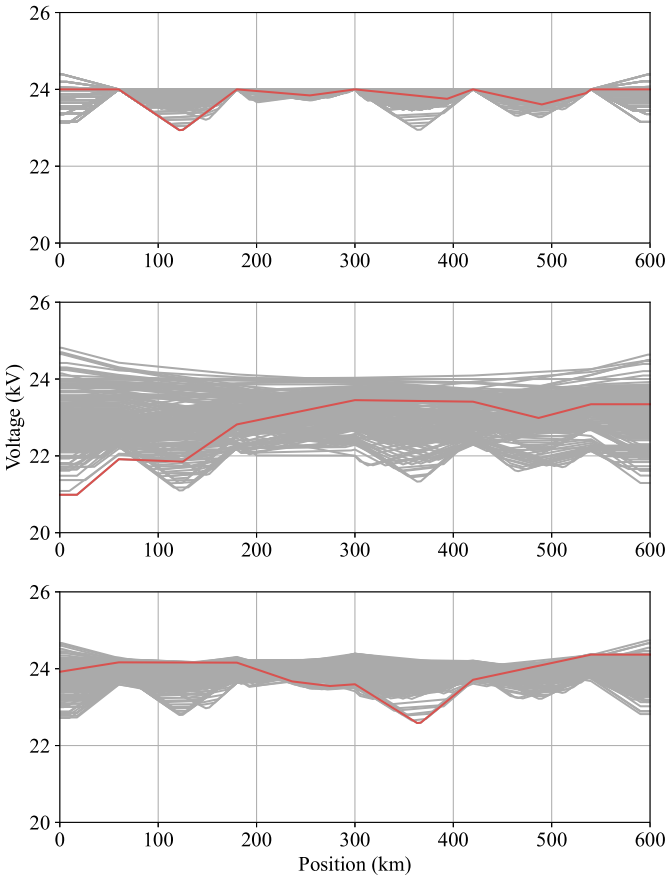

Fig. 4. Normal operation: voltage profiles along the railway system during the simulated period with the minimum (red/solid) voltages. (Top) *FV* approach. (Mid) *LD* approach. (Bottom) *CONS* approach.

Table 2
Catenary voltage statistical results for normal operation.

Control strategy	FV	LD	CONS
Mean (kV)	23.91	23.02	23.90
Median (kV)	24.00	23.03	23.94
Minimum (kV)	22.91	20.90	22.54
Maximum (kV)	24.41	24.85	24.76
95% conf. int. (kV)	[23.52, 24.25]	[21.91, 24.13]	[23.38, 24.43]

One of the main advantages of the proposed multi-terminal DC railway electrification is the possibility of sharing the traction load among the set of VSC power stations. This may lead, in conjunction with adequate control actions, to a much lower power rating of the substation assets. The influence of the controller in the load sharing can be assessed by analyzing the substation power injections, represented in Fig. 6 through box plots. In the case of the *FV* approach, the power delivered by the VSC substation depends on the demand of the rolling stock and its relative position with respect to the substation, since the supply voltage is kept constant. As a result, large variations in the injected power occur, as shown in Fig. 6. This leads to large maximum injected power (about 13.4 MW), owing to the reduced load-sharing capability of this control approach. In contrast, the *LD* strategy leads to lower active power variations, and hence reduced maximum active power injections (about 8.8 MW), because the load is shared among the different substations irrespective of the train positions. Nevertheless, this good performance is achieved to the detriment of the voltage profiles, as previously discussed with the help of Fig. 5. The incorporation of the secondary consensus-based controller, as an

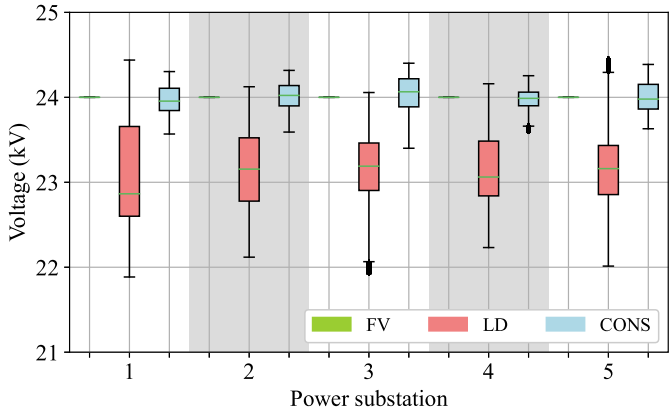

Fig. 5. Normal operation: box plots of the VSC DC output voltages at each power station during the simulated period.

Table 3
Power, energy, losses and efficiency results for normal operation.

Control strategy	FV	LD	CONS
Maximum power (MW)	13.4	8.8	9.6
VSC rated power (MW)	19.9	15.6	15.5
Trains energy (MWh)	107.77	107.77	107.77
AC energy (MWh)	114.00	113.82	113.41
Catenary losses (MWh)	1.70	2.39	2.03
Converter losses (MWh)	4.52	3.65	3.61
Total losses (MWh)	6.22	6.04	5.64
Efficiency	94.5	94.7	95.0

enabler of the load sharing capabilities to simultaneously reducing the voltage variations, yields excellent results. In this respect, note that, even though the maximum power demand reaches 9.6 MW under the *CONS* approach, the median and interquartile ranges of the VSC power injections are almost the same as those of the *LD* controller. This reveals that the performance of the proposed *CONS* algorithm is similar to the best controller in terms of the load sharing KPI.

Table 3 summarizes the main simulation results for the normal scenario where all the VSC stations are in operation. These include maximum VSC powers, energy losses, efficiency and VSC rated power. It is worth noting that the VSC ratings are defined according to the results detailed in Section 5.2, where a scenario with a faulted substation is analyzed. In this regard, the higher VSC rating is associated to the *FV* control approach, due to its inherent inability to provide load sharing. In contrast, due to the ability to keep the supply voltages constant, the *FV* controller achieves the lowest catenary ohmic losses. However, the larger VSC rating required by this controller penalizes the converter losses. As a result, the *FV* control approach will lead to the higher CAPEX and OPEX, since it requires the use of large VSCs which reduce the overall system efficiency. Conversely, the *LD* controller achieves the lowest VSC rated power, with a positive impact on the CAPEX. However, the catenary losses considerably increase, since the load is shared among all the VSC substations while the catenary voltages are lower, as shown in Fig. 5. In any case, the overall system efficiency increases due to the lower VSC losses. Finally, the proposed *CONS* approach leads to VSC ratings that are almost the same as in the *LD* controller, achieving the best overall efficiency. This is due to the improved voltage profile, which reduces the ohmic losses of the catenary with respect to the *LD* controller.

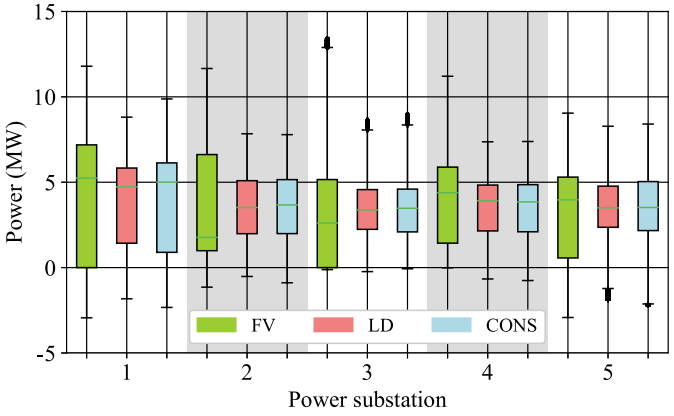

Fig. 6. Normal operation: box plot of the VSC substation injected power during the simulated period.

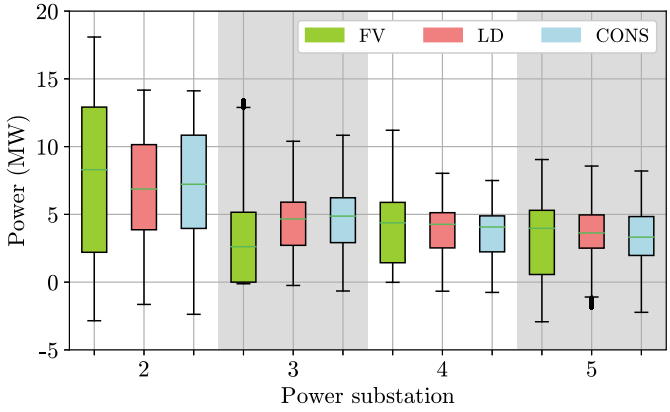

Fig. 7. Worst-case faulted operation: box plot of the VSC substation injected power during the simulated period.

Table 4
Simulation results with a single faulted VSC substation.

VSC out	V_{min} (kV)			P_{max} (MW)		
of service	FV	LD	CONS	FV	LD	CONS
VSC1	18.91	14.19	17.84	18.1	14.2	14.1
VSC2	21.88	19.48	20.73	14.5	11.2	10.8
VSC3	21.93	19.55	21.24	14.1	10.6	9.8
VSC4	22.24	20.06	21.22	16.5	11.8	11.2
VSC5	20.39	16.67	18.55	16.8	14.5	12.4

5.2. Operation with faulted VSC substation

This section is devoted to an analysis of a faulted scenario where a VSC substation remains disconnected due to an outage while the respective communication links become idling. Table 4 shows, for each control strategy, the minimum voltage along the catenary and the maximum power provided by the VSCs in service. Each substation outage has been considered to last for the entire simulated period and, thus, the trains are fed by the four remaining substations. From Table 4, it can be concluded that the worst-case scenario corresponds to an outage at the VSC substation 1, as it leads to the minimum catenary voltage and the maximum active power demand. Note that this active power value determines the rated power of the VSC substations included in Table 3, where a 20% safety margin has been applied. The overload of the VSC substation during faulty conditions forces injected peak powers greater than 18 MW when the *FV* strategy is applied. However, by applying the *CONS* controller, the power is shared among the VSC substations, much like in the *LD* approach as shown in Fig. 7.

Fig. 8 shows the catenary voltages over the simulated time period, clearly evidencing that the lower voltages arise in the surroundings of the faulted substation. The statistical analysis of the catenary voltages is presented in Table 5. These results show that the *CONS* strategy maintains the minimum voltage at 17.84 kV (0,74 p.u.), which is close to the 18.91 kV (0.79 p.u.) achieved by the *FV* approach. The comparison is even better regarding the 95% confidence intervals, where the voltage differences are below 2% ([0.91–1.04] p.u. for the *FV* scheme versus [0.90–1.06] p.u. for the proposed *CONS* control). On the contrary, the *LD* controller leads to unacceptable minimum voltage, which reaches 14.19 kV (0.59 p.u.), while the 95% confidence interval for the catenary voltage is also wider: [0.82–1.05] p.u.

5.3. Influence of controller gains

As the two main objectives of the controller, namely voltage regulation and load sharing, are contradictory to a large extent, it is worth exploring the sensitivity of the system performance to the controller gains.

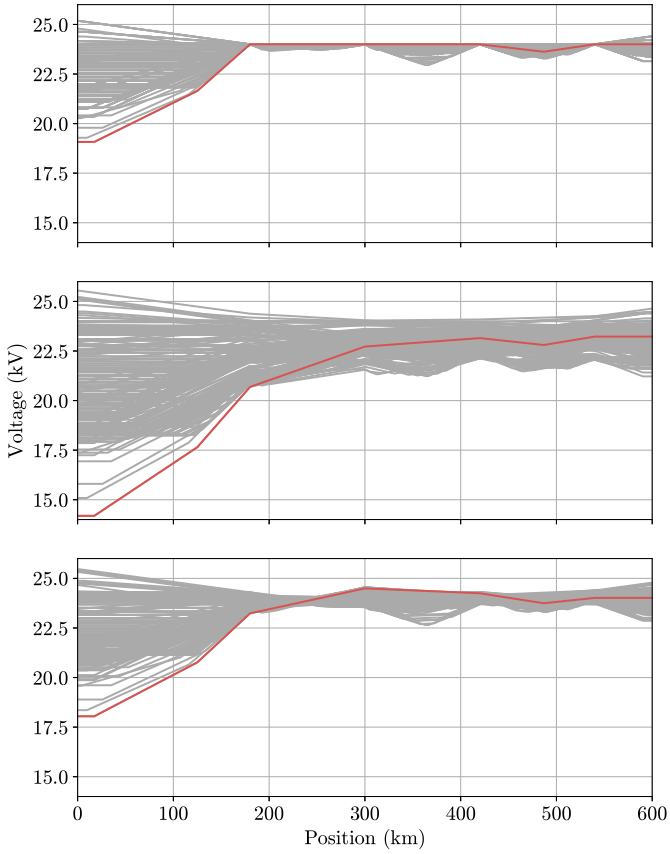

Fig. 8. Worst-case faulted operation: voltage profiles along the railway system during the simulated period with the minimum (red/solid) voltages. (Top) *FV* approach. (Mid) *LD* approach. (Bottom) *CONS* approach.

Table 5
Catenary voltage statistical results for the worst-case faulted operation.

Control strategy	FV	LD	CONS
Mean (kV)	23.70	22.43	23.65
Median (kV)	23.98	22.76	23.90
Minimum (kV)	18.91	14.19	17.84
Maximum (kV)	25.21	25.59	25.50
95% conf. int. (kV)	[22.04, 25.04]	[19.68, 25.18]	[21.66, 25.39]

For this purpose, simulations are carried out using the normal operation scenario, and the results are summarized in Table 6. The

Table 6
Sensitivity of the system performance to controller gains.

K_s	a_{ij}	$\|\Delta V\|^{max}_{VSC}$ (V)	$\|\Delta V\|^{max}_{cat}$ (V)	$\|P\|^{max}_{VSC}$ (MW)
1.35	0.10	590	1602	9.10
2.7	**0.10**	**387**	**1455**	**9.88**
5.4	0.10	260	1327	10.54
2.7	0.02	134	1207	11.31
2.7	**0.10**	**1455**	**387**	**9.88**
2.7	0.50	978	2024	8.05

KPIs shown in this table correspond to the maximum voltage deviation with respect to the rated voltage at the VSC output ($|\Delta V|^{max}_{VSC}$) and the catenary ($|\Delta V|^{max}_{cat}$), respectively, as well as the maximum power injected by any of the VSC stations (P^{max}_{VSC}). The first two KPIs are related to the voltage regulation capability, while the third is indicative of the load sharing feature.

The rows of Table 6 corresponding to the base-case parameters used in the simulations discussed in the previous sections (i.e., $K_s = 2.7$ and $a_{ij} = 0.1$), are highlighted in bold font. First, the upper part of the table compares the results when only the value of the gain K_s is altered. This variable is increased and decreased by a factor of two. As expected, the reduction of this parameter causes a greater deviation of the voltages with respect to the rated value. In contrast, increasing this parameter means that the voltage is kept within a narrower band. The consequence of limiting the voltage deviation is a reduction in power-sharing ability and, therefore, an increase of the maximum power injected by a station. A similar discussion can be made with the bottom of the table, where the value of a_{ij} has been changed by a factor of five. However, note that changing the value of one of the gains affects both targets. Thus, in addition to the value of the gain itself, it is necessary to consider the relative values between them.

6. Conclusion

This paper has proposed a distributed control approach based on the consensus concept to control the VSCs that feed a MTDC railway electrification system. The controller relies on a simple communication infrastructure that takes advantage of the particular topology of the underlying railway system. Each VSC substation shares information with its adjacent neighbors to define the corresponding operating point, which is defined by a consensus-based algorithm. The aim of the underlying control law is to simultaneously balance the two main objectives of any MTDC system, namely: voltage regulation and power-sharing among the VSCs feeding the DC grid. As a matter of fact, purely local control strategies fail in this purpose. On the one hand, the trivial strategy of keeping constant the VSC terminal voltage, irrespective of the train locations, leads to the flattest voltage profile and lowest catenary circulating currents, at the cost of higher VSC ratings due to inefficient VSC power-sharing. On the other hand, the conventional droop controller achieves a good load balance, reducing accordingly the substation installed power, but voltage drops are noticeably higher. The proposed consensus-based distributed load-sharing provides a weighted compromise solution: load-sharing is improved by letting VSCs help their neighbors while the voltage profiles are not subject to severe fluctuations. In addition, the efficiency is slightly improved when overall losses (i.e. VSC substations plus the catenary) are considered. All these advantages are obtained with a distributed control scheme that relies on the simplest communication infrastructure, in contrast to a fully centralized paradigm, which facilitates its field deployment and operational robustness.

Declaration of competing interest

The authors declare that they have no known competing financial interests or personal relationships that could have appeared to influence the work reported in this paper.

Data availability

All the used data are within the paper.

Acknowledgments

The authors would like to thank the financial support of the Spanish Ministry of Science and Innovation and Junta de Andalucía through the projects PID2021-124571OB-I00 and FLEX-REN (P18-TP-3655) respectively. Financial support for this research was also provided by the CERVERA research programme of CDTI, the Industrial and Technological Development Centre of Spain, under the research Project HySGrid+ (CER-20191019). J. Carlos Olives would like to thank University of Seville in the framework of the VI PPIT-US for supporting his research.

Appendix

The power losses that have been considered in this work refer to the VSC, the substation transformer, and the auxiliary services. The resulting values collected in Table 1 are justified as follows:

- VSC. The VSC used in this application corresponds to an MMC topology. The MMC losses strongly depend on several factors, e.g. submodule configuration and voltage balancing algorithms, among others [36]. In [37] converter losses around 1% are obtained for a 1-GW MMC. In [38], for a nominal power of 25 MW (closer to the proposed in our paper), the losses are estimated to be around 1.7%. In this paper, no distinction is made between no-load losses and total full-load losses. In [39], a 5-MW half-bridge MMC is reported to have 0.4% conduction losses and 0.22% switching losses, giving a full-load losses of 0.62%. These power losses are relatively low compared to other reported results, but they give a hint that switching losses in a medium-voltage and medium-power MMC are half of the conduction losses. Taking all these issues into account, the total power losses are assumed to be 1.25%, between the values proposed by [37,38], where the no-load and full-load conduction losses are 0.42% and 0.84%, respectively.
- Transformer. The total power losses of the transformer have to fulfill the current energy efficiency standard [40]. For this reason, a minimum peak efficiency of 99.7% has been considered given the characteristic rated power of the substation transformer, which is about 25 MVA. Note that the maximum efficiency of the transformer corresponds to a load factor given by the relationship between the no-load (P_o) and Joule full-load (P_{cu}) power losses: $C_{opt} = \sqrt{P_o/P_{cu}}$. Therefore, it is possible to derive the power losses terms given the load factor for the maximum transformer efficiency. The load factor of the substation transformers has been considered to be about 80%, which is a high value since the objective of the proposed secondary control algorithm is to share the traction power to reduce the VSC ratings as much as possible. As a result, the no-load losses and full-load Joule losses are estimated as 0.15% and 0.23% respectively.
- Auxiliary services. Cooling systems, ICT devices, and other substation components demand active power, which has been estimated to be 0.1% of the rated power.

References

[1] IEA. The future of rail. Tech. rep., IEA; 2019.
[2] Arboleya P, Bidaguren P, Armendariz U. Energy is on board: Energy storage and other alternatives in modern light railways. IEEE Electrif Mag 2016;4(3):30–41. http://dx.doi.org/10.1109/MELE.2016.2584938.
[3] Krastev I, Tricoli P, Hillmansen S, Chen M. Future of electric railways: Advanced electrification systems with static converters for ac railways. IEEE Electrif Mag 2016;4(3):6–14. http://dx.doi.org/10.1109/MELE.2016.2584998.

[4] Giannakis A, Peftitsis D. Performance evaluation and limitations of overvoltage suppression circuits for low- and medium-voltage DC solid-state breakers. IEEE Open J Power Electron 2021;2:277–89. http://dx.doi.org/10.1109/OJPEL.2021.3068531.

[5] Dai NY, Lao K-W, Lam C-S. Hybrid railway power conditioner with partial compensation for converter rating reduction. IEEE Trans Ind Appl 2015;51(5):4130–8. http://dx.doi.org/10.1109/TIA.2015.2426134.

[6] Li D, Zouma A, Liao J-T, Yang H-T. An energy management strategy with renewable energy and energy storage system for a large electric vehicle charging station. eTransportation 2020;6:100076. http://dx.doi.org/10.1016/j.etran.2020.100076.

[7] Brenna M, Foiadelli F, Kaleybar HJ, Fazel SS. Smart electric railway substation using local energy hub based multi-port railway power flow controller. In: 2019 IEEE vehicle power and propulsion conference. VPPC, 2019, p. 1–6. http://dx.doi.org/10.1109/VPPC46532.2019.8952414.

[8] Brenna M, Foiadelli F, Kaleybar HJ. The evolution of railway power supply systems toward smart microgrids: The concept of the energy hub and integration of distributed energy resources. IEEE Electrif Mag 2020;8(1):12–23. http://dx.doi.org/10.1109/MELE.2019.2962886.

[9] Arboleya P, Mohamed B, El-Sayed I. DC railway simulation including controllable power electronic and energy storage devices. IEEE Trans Power Syst 2018;33(5):5319–29. http://dx.doi.org/10.1109/TPWRS.2018.2801023.

[10] Aguado JA, Sánchez Racero AJ, de la Torre S. Optimal operation of electric railways with renewable energy and electric storage systems. IEEE Trans Smart Grid 2018;9(2):993–1001. http://dx.doi.org/10.1109/TSG.2016.2574200.

[11] Arboleya P, Mohamed B, El-Sayed I. Off-board and on-board energy storage versus reversible substations in DC railway traction systems. IET Electr Syst Transp 2020;10(2):185–95. http://dx.doi.org/10.1049/iet-est.2019.0022.

[12] Xu Q, Ma F, He Z, Chen Y, Guerrero JM, Luo A, Li Y, Yue Y. Analysis and comparison of modular railway power conditioner for high-speed railway traction system. IEEE Trans Power Electron 2017;32(8):6031–48. http://dx.doi.org/10.1109/TPEL.2016.2616721.

[13] Kaleybar HJ, Kojabadi HM, Brenna M, Foiadelli F, Fazel SS. An active railway power quality compensator for 2x25kV high-speed railway lines. In: 2017 IEEE international conference on environment and electrical engineering and 2017 IEEE industrial and commercial power systems Europe (EEEIC / I CPS Europe). 2017, p. 1–6. http://dx.doi.org/10.1109/EEEIC.2017.7977679.

[14] Ma F, Wang X, Deng L, Zhu Z, Xu Q, Xie N. Multiport railway power conditioner and its management control strategy with renewable energy access. IEEE J Emerg Sel Top Power Electron 2020;8(2):1405–18. http://dx.doi.org/10.1109/JESTPE.2019.2899138.

[15] Arboleya P, Mayet C, Mohamed B, Aguado JA, de la Torre S. A review of railway feeding infrastructures: Mathematical models for planning and operation. eTransportation 2020;5:100063. http://dx.doi.org/10.1016/j.etran.2020.100063.

[16] Leander P, Ostlund S. A concept for an HVDC traction system. In: Main line railway electrification, 1989., International conference on. 1989, p. 169–73.

[17] Gomez-Exposito A, Mauricio JM, Maza-Ortega JM. VSC-based MVDC railway electrification system. IEEE Trans Power Deliv 2014;29(1):422–31. http://dx.doi.org/10.1109/TPWRD.2013.2268692.

[18] Simiyu P, Xin A, Bitew GT, Shahzad M, Kunyu W, Tuan LK. Review of the DC voltage coordinated control strategies for multi-terminal VSC-MVDC distribution network. J Eng 2019;2019(16):1462–8. http://dx.doi.org/10.1049/joe.2018.8841.

[19] Gavriluta C, Candela JI, Citro C, Rocabert J, Luna A, Rodríguez P. Decentralized primary control of MTDC networks with energy storage and distributed generation. IEEE Trans Ind Appl 2014;50(6):4122–31. http://dx.doi.org/10.1109/TIA.2014.2315715.

[20] Yang X, Hu H, Ge Y, Aatif S, He Z, Gao S. An improved droop control strategy for VSC-based MVDC traction power supply system. IEEE Trans Ind Appl 2018;54(5):5173–86. http://dx.doi.org/10.1109/TIA.2018.2821105.

[21] Guerrero JM, Vasquez JC, Matas J, de Vicuna LG, Castilla M. Hierarchical control of droop-controlled AC and DC microgrids - A general approach toward standardization. IEEE Trans Ind Electron 2011;58(1):158–72. http://dx.doi.org/10.1109/TIE.2010.2066534.

[22] Nasirian V, Shafiee Q, Guerrero JM, Lewis FL, Davoudi A. Droop-free distributed control for AC microgrids. IEEE Trans Power Electron 2016;31(2):1600–17. http://dx.doi.org/10.1109/TPEL.2015.2414457.

[23] Aatif S, Hu H, Yang X, Ge Y, He Z, Gao S. Adaptive droop control for better current-sharing in VSC-based MVDC railway electrification system. J Mod Power Syst Clean Energy 2019;7(4):962–74. http://dx.doi.org/10.1007/s40565-018-0487-0.

[24] Sharifi S, Kamel T, Tricoli P. Investigating the best topology for traction power substations (TPSs) in a medium voltage DC (MVDC) railway electrification system. In: 2021 23rd European conference on power electronics and applications (EPE'21 ECCE Europe). 2021, p. 1–10. http://dx.doi.org/10.23919/EPE21ECCEEurope50061.2021.9570403.

[25] Ferreira JA. The multilevel modular DC converter. IEEE Trans Power Electron 2013;28(10):4460–5. http://dx.doi.org/10.1109/TPEL.2012.2237413.

[26] Debnath S, Qin J, Bahrani B, Saeedifard M, Barbosa P. Operation, control, and applications of the modular multilevel converter: A review. IEEE Trans Power Electron 2015;30(1):37–53. http://dx.doi.org/10.1109/TPEL.2014.2309937.

[27] Nasirian V, Moayedi S, Davoudi A, Lewis F. Distributed cooperative control of DC microgrids. IEEE Trans Power Electron 2015;30(4):2288–303. http://dx.doi.org/10.1109/TPEL.2014.2324579.

[28] Choi H, Jung J. Enhanced power line communication strategy for DC microgrids using switching frequency modulation of power converters. IEEE Trans Power Electron 2017;32(6):4140–4. http://dx.doi.org/10.1109/TPEL.2017.2648848.

[29] Anand S, Fernandes BG, Guerrero JM. Distributed control to ensure proportional load sharing and improve voltage regulation in low-voltage DC microgrids. IEEE Trans Power Electron 2013;28(4):1900–13. http://dx.doi.org/10.1109/TPEL.2012.2215055.

[30] Bidram A, Davoudi A. Hierarchical structure of microgrids control system. IEEE Trans Smart Grid 2012;3(4):1963–76. http://dx.doi.org/10.1109/TSG.2012.2197425.

[31] Dehkordi NM, Sadati N, Hamzeh M. Robust tuning of transient droop gains based on Kharitonov's stability theorem in droop-controlled microgrids. IET Gener Transm Distrib 2018;12(14):3495–501. http://dx.doi.org/10.1049/iet-gtd.2017.1767.

[32] Serrano-Jiménez D, Castano-Solís S, Unamuno E, Barrena J. Droop control operation strategy for advanced DC converter-based electrical railway power supply systems for high-speed lines. Int J Electr Power Energy Syst 2022;137:107870. http://dx.doi.org/10.1016/j.ijepes.2021.107870.

[33] Olfati-Saber R, Fax JA, Murray RM. Consensus and cooperation in networked multi-agent systems. Proc IEEE 2007;95(1):215–33. http://dx.doi.org/10.1109/JPROC.2006.887293.

[34] Lewis FL, Zhang H, Hengster-Movric K, Das A. Cooperative control of multi-agent systems: Optimal and adaptive design approaches. Springer Publishing Company, Incorporated; 2014.

[35] Aatif S, Hu H, Rafiq F, He Z. Analysis of rail potential and stray current in MVDC railway electrification system. Railw Eng Sci 2021;29:394–407. http://dx.doi.org/10.1007/s40534-021-00243-0.

[36] Tian Y, Wickramasinghe H, Li Z, Pou J, Konstantinou G. Review, classification and loss comparison of modular multilevel converter submodules for HVDC applications. Energies 2022;15(6):1985. http://dx.doi.org/10.3390/en15061985.

[37] Rohner S, Bernet S, Hiller M, Sommer R. Modulation, losses, and semiconductor requirements of modular multilevel converters. IEEE Trans Ind Electron 2010;57(8):2633–42. http://dx.doi.org/10.1109/TIE.2009.2031187.

[38] Gnanarathna UN, Gole AM, Rajapakse AD, Chaudhary SK. Loss estimation of modular multi-level converters using electro-magnetic transients simulation. In: Proc. int. conf. power syst. transient. IPST, 2011, p. 1–6.

[39] Zeng R, Xu L, Yao L, Williams BW. Design and operation of a hybrid modular multilevel converter. IEEE Trans Power Electron 2015;30(3):1137–46. http://dx.doi.org/10.1109/TPEL.2014.2320822.

[40] Regulation (EU) No 548/2014 on implementing Directive 2009/125/EC of the European Parliament and of the Council with regard to small, medium and large power transformers. European Commission; 2019.